Tectonophysics 762 (2019) 159–168

Contents lists available at ScienceDirect

Tectonophysics

journal homepage: www.elsevier.com/locate/tecto

Source parameter analysis of microearthquakes recorded around the underground gas storage in the Montello-Collalto Area (Southeastern Alps, Italy)

L. Moratto[a,*], M.A. Romano[a], G. Laurenzano[a], S. Colombelli[b], E. Priolo[a], A. Zollo[b], A. Saraò[a], M. Picozzi[b]

[a] Istituto Nazionale di Oceanografia e di Geofisica Sperimentale - OGS, Borgo Grotta Gigante 42c, 34010 Sgonico, Trieste, Italy
[b] Università di Napoli "Federico II", Dipartimento di Fisica Ettore Pancini, Via Cinthia, 21, 80126 Napoli, Italy

ARTICLE INFO

Keywords:
Microseismicity
Source parameters
Moment magnitude (M_W)
Underground Gas Storage (UGS)
Northeastern Italy
Southeastern Alps

ABSTRACT

The study of seismic source parameters is crucial for understanding the origin of seismicity and retrieving information on the energy balance and the stress involved in earthquake rupture processes. In active tectonic areas, where underground industrial activities are carried out, such parameters may help to understand whether earthquakes are induced, triggered, or natural. The Montello-Collalto area (Southeastern Alps) is located in an active tectonic environment and hosts a depleted natural reservoir used to store gas. Since 2012, a high-quality seismic network monitors the microseismicity occurring around the underground gas storage reservoir to understand if the storage activity might induce seismicity. In this paper, we estimate the source parameters of low magnitude events representative of the seismicity occurring in the area surrounding the reservoir. The analysis includes a preliminary removal of the site effects, specifically computed within this study, from all the records. Then, using a parametric multistep inversion scheme, we estimate the seismic moment, the corner frequency and the static stress drop, that can be set as reference for the microseismicity occurring in the study area. All the investigated earthquakes show low seismic efficiency compatible with overshoot processes, which is typical of natural (i.e., tectonic) earthquakes. Our procedure can be implemented in other tectonic regions hosting underground industrial activities to support the decisional processes related to real-time monitoring.

1. Introduction

The accurate estimation of the hypocentral location, magnitude, and source parameters for microearthquakes occurring in the surroundings of areas exploited for subsurface industrial purposes is a crucial task for discriminating between natural and anthropogenic events (Hua et al., 2013; Grigoli et al., 2017). The level of accuracy that is possible to reach depends on three main factors: i) the network capability to detect and accurately locate microseismicity; ii) the availability of robust models for the correction of site and path attenuation effects on recording; and iii) the approach adopted to estimate the microearthquake source parameters. Accurate microseismicity location allows to map the spatiotemporal evolution of the seismicity which could reflect underground fluid migrations (Ogwari et al., 2016). Goertz-Allmann et al. (2011) correlated the stress drop with pore pressure perturbations due to the injection at the Basel (Switzerland) geothermal site. Husen et al. (2013) estimated the source dimension to identify the fault patch that repeatedly ruptured during the excavation of the Gotthard Base Tunnel in Switzerland. Picozzi et al. (2017) investigated the induced earthquakes related to geothermal fields observing that events gather in various clusters with similar source parameters and that smaller and larger events have different dynamic processes. The most advanced discrimination methods, whether statistics- or physics-based, rely on accurate locations and use source parameters estimated from observed data (e.g., Grigoli et al., 2017, for a review).

In Italy, the Italian government has issued guidelines for monitoring the seismicity in areas surrounding underground industrial activities (MiSE, 2014) after the 2012 Emilia (Italy) seismic sequence. Indeed, the possibility that the sequence was triggered by industrial activities (ICHESE, 2014) gave rise to strong controversies at both the public and political levels (Grigoli et al., 2017) leading to a halt in new hydrocarbon leases. The Italian guidelines require implementing high-quality monitoring systems to track the space-time evolution of the

* Corresponding author.
E-mail address: lmoratto@inogs.it (L. Moratto).

https://doi.org/10.1016/j.tecto.2019.04.030
Received 16 November 2018; Received in revised form 10 April 2019; Accepted 25 April 2019
Available online 27 April 2019

microseismicity and refining the databases of the monitored parameters by including the estimate of the moment magnitude and, in general, a more detailed source parameterization.

In line with such recommendations, the Istituto Nazionale di Oceanografia e di Geofisica Sperimentale - OGS has designed a high-sensitivity network with the aim of monitoring the underground gas storage (UGS) activity carried out in the depleted gas reservoir of Collalto (Northeastern Italy) and providing highly accurate locations of the seismicity occurring near the reservoir (Priolo et al., 2015a). The area under study is located in the foothills of the Southeastern Alps, close to seismogenic faults capable of generating strong earthquakes ($M_W \geq 6$) (e.g., Burrato et al., 2008). For this reason, the Collalto site represents an emblematic example of underground industrial activities carried out in a tectonic environment that must face a high social demand for assessing and mitigating the seismic risk, a task which requires the capability of tracking the background seismicity with high resolution (Romano et al., 2019). A further peculiarity of this study is that UGS in depleted natural gas reservoirs with pressure not exceeding the original gas pressure may be considered an exception to the assumption that fluids (in this case gas) injected at depth usually produce seismicity; indeed, for this specific kind of activity there are only a few of documented cases of induced seismicity and they concern only micro- or, better, nano-seismicity close to the injection wells within the reservoirs (Evans, 2008).

In this study, we use a set of weak earthquakes well recorded in the Collalto area to test and validate a procedure that provides robust estimations of the moment magnitude (M_W; Kanamori, 1977; Hanks and Kanamori, 1979) and other source parameters for the monitoring system developed there. The seismic source parameters for weak events are generally estimated considering kinematic (Brune, 1970) or dynamic (Madariaga, 1976) source models of the body-wave displacement spectrum. In particular, the adoption of the ω^2 source displacement spectrum allows the estimation of the seismic moment (M_0, i.e., used in turn to calculate M_W) and the corner frequency (f_c), which combined with M_0 allows obtaining the source radius and the associated stress drop. However, to determine source parameters is not an easy task, and deviation from the simple ω^2 point-source model (Kaneko and Shearer, 2015; Uchide and Kazutoshi, 2016) or limitation in the high-frequency bandwidth (Abercrombie, 2015) can result in relevant uncertainties associated to the investigated source parameters.

With the growth of dense digital networks and the availability of high-quality spectra also for microearthquakes, M_W is increasingly computed for estimating the magnitude of weak earthquakes, although it was developed for estimating the size of moderate to strong earthquakes (Bormann et al., 2013). This parameter is of particular importance in seismic hazard assessment, not only for improving knowledge of the natural seismicity occurring in active fault regions (Zollo et al., 2014) but also for gaining deeper insight into the microearthquakes induced by human activities (Picozzi et al., 2017).

Another important source parameter is the radiated seismic energy (Er), which can be computed from the velocity waveforms (e.g., among others, Kanamori et al., 1993; Bindi et al., 2018); the relation of Er with the seismic moment provides the apparent stress (Choy and Boatwright, 1995), which is a proxy for the dynamic stress release (Boatwright, 1988). Furthermore, the ratio between the apparent stress and the static stress drop provides the seismic efficiency (Beeler et al., 2003), which gives information about the energy radiated in relation to the global energy available for the rupture process.

Recently, Moratto et al. (2017) computed the seismic moment for a large set of low magnitude ($M_W \leq 4.0$) earthquakes that occurred in Northeastern Italy. However, the adopted approach did not provide estimates of the corner frequencies of the events and consequently of other seismic source parameters. A method developed by Zollo et al. (2014) allows both investigating the attenuation effects that contribute to modify the seismic source spectrum of earthquakes and estimating the seismic source parameters by a multistep, nonlinear inversion strategy. The method has been efficiently applied for studying the microseismicity associated with the fault system responsible for the 23 November 1980, MS 6.9, Irpinia earthquake (Ameri et al., 2011).

A known problem in source parameter studies, which becomes even more relevant in the case of microearthquakes, is the influence of the site effects, since they can alter the shape of the seismic spectra at frequencies comparable to the corner frequency (see for example: Frankel, 1982; Hanks, 1982; Frankel and Wennerberg, 1989; Tusa et al., 2006). Therefore, an appropriate spectral correction of the site effects is crucial when assessing source parameters.

In this paper, we integrate the Zollo et al. (2014) method with the site effects estimates available for the Collalto area and apply this modified approach to a subset of 30 selected microearthquakes; these events are highly representative of the 5-year seismicity recorded around the Collalto reservoir area, with magnitudes and depths in the range $1 \leq M_L \leq 3$ and 5–15 km, respectively. In the following, after describing the method and the preliminary data processing to remove the site effects, we discuss the results. Following the calibration and validation performed in this study, the presented procedure is ready for being implemented within the standard routine analyses for the rapid characterization of the Collalto seismicity. Moreover, our approach can be easily applied to other tectonically active areas where underground activities take place.

2. Dataset and processing

The Collalto UGS reservoir, managed since 1994 by Edison Stoccaggio S.p.A., is located in the foothills of the Southeastern Alps (Northeastern Italy) close to the Montello hill (Fig. 1a), where some seismogenic faults are recognized (Burrato et al., 2008). During the past centuries, this area has been stricken by moderate-strong earthquakes ($5.0 \leq M_W \leq 6.4$) (Rovida et al., 2016), while it is currently affected only by minor seismicity ($M \leq 4$), and characterized by a medium-high level of seismic hazard (0.25–0.30 g with 10% probability of exceedance in 50 years; GdL MPS, 2004).

The reservoir is a depleted natural gas deposit, approximately 8 km long and 1.5 km wide, managed according to seasonal cycles of gas extraction during the winter, and gas injection during the summer at a pressure of 160 bars close to the original pressure. Since 2012, the seismicity around the reservoir has been monitored by the Collalto Seismic Network (OGS, 2012) —international code EV; EV network hereinafter— which is composed of 10 stations (Priolo et al., 2015a) mainly located on Plio-Pleistocene clays (Avigliano et al., 2008) at the northern margin of the Venetian Plain (Fig. 1a). Nine stations are equipped with borehole seismometers with extended period ($T = 10$ s or $T = 30$ s) and one with a broad-band seismometer ($T = 120$ s), in continuous data acquisition at 200 Hz. Stations are dense just above the reservoir, in the so-called area A (where induced microseismicity could occur), and become sparser moving away from it (Fig. 1a). To improve the earthquake location in a large area around the reservoir, here indicated as area B, the EV network recordings are routinely integrated with data recorded by other stations belonging to nearby seismic networks (Fig. 1a). The average station interdistance is 4 and 10 km in area A and B, respectively. More than 1000 events where recorded during the first five years of monitoring (2012–2016): 432 located in area A with $-1.8 \leq M_L \leq 3.7$ and 555 located in area B (outside of area A) with $-0.3 \leq M_L \leq 3.8$ (Fig. 1a). Earthquake locations and M_L estimates (Bragato and Tento, 2005) are performed using the standard procedure of the OX-North-East Italy seismic network (OGS, 2016). All the detected events are automatically processed in real time and then manually reviewed in the following days before to be listed in the Online preliminary catalog (http://rete-collalto.crs.inogs.it; 2018).

In Italy, only naturally depleted gas reservoirs are allowed for UGS. For this type of activity, the Italian Guidelines (MiSE, 2014) indicate that microearthquakes ($M < 2$), possibly induced by local stress changes associated with the gas injection/extraction activity, can occur

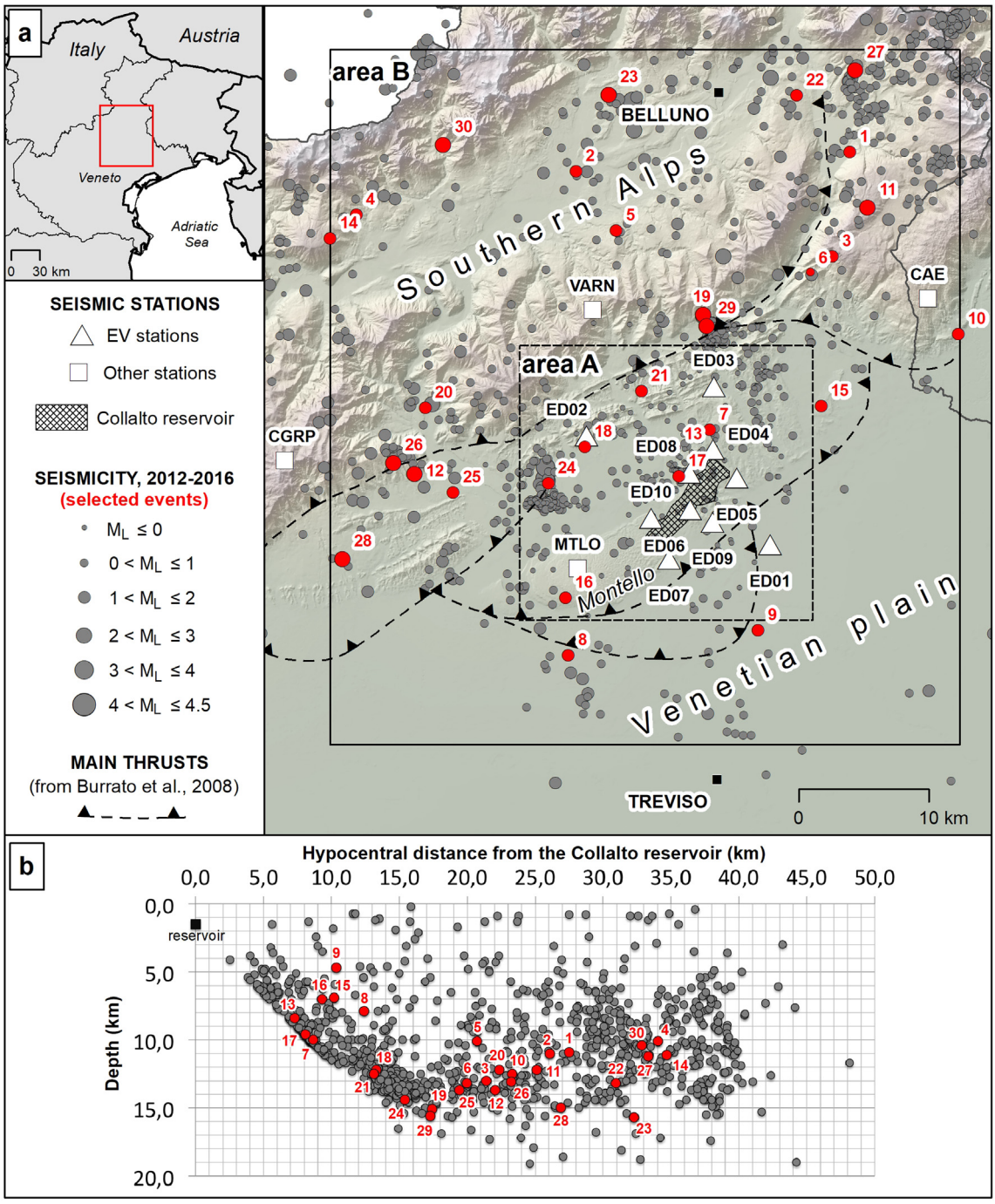

Fig. 1. a) Epicentral map of earthquakes recorded by the EV network in the period 2012–2016 (gray circles); the 30 events selected for this study (Table 1) are plotted in red. b) Depth versus hypocentral distance from the Collalto reservoir for earthquakes recorded by the EV network (gray circles); red symbols as above.

at a limited distance (i.e., within 3 km) from the reservoir. We observe that all the hypocenters recorded by the EV network, except one, are more than 3 km away from the gas reservoir edges and more than 90% of them are located between 5 and 15 km depth, much deeper than the gas reservoir bottom (Fig. 1b). Based on these observations, we infer that these events are not directly caused by the industrial operations at the UGS facility. Moreover, under area A, the seismicity clearly depicts a NW-dipping surface, which corresponds well to one of the thrust faults recognized in the area (Fig. 1a, Burrato et al., 2008), suggesting a more likely tectonic origin for the earthquakes (Romano et al., 2015). The natural origin of the local seismicity is further strengthened by the very low correlation value (about 0.2) found between wellhead gas-pressure and seismicity rate using the Oprsal e Eisner (2014) approach.

For the aim of this study, we selected a set of events for which high-quality waveform records have been acquired. The selection was based on the following three criteria: $1 \leq M_L \leq 3$, different source-receiver distances and wide coverage of the study area. The resulting set is composed of 30 events that represent the local microseismicity (Fig. 1a). Details about their location parameters are specified in Table 1; on the whole, these earthquake locations feature on average (± first standard deviation) RMS = 0.20 ± 0.08 s, statistical horizontal error ErrH = 0.6 ± 0.2 km and vertical error ErrV = 1.0 ± 0.6 km, GAP = 114 ± 62 and minimum 10 P + 6 S phase readings. For each selected event, we extracted all the waveforms that

Table 1
Detailed location parameters and magnitudes of the 30 earthquakes selected from the EV catalog and analyzed in this study (see Fig. 1).

ID	Area	Date	Origin time (UTC)	Lat (dd)	Lon (dd)	Depth (km)	M_L	GAP	#P	#S	ErrH (km)	ErrV (km)	RMS (s)
1	B	2012/01/07	12:02:40.78	46.109	12.355	10.9	1.1	116	13	9	0.6	1.4	0.22
2	B	2012/01/08	17:30:18.79	46.089	12.083	11.0	1.8	67	21	8	0.7	1.5	0.28
3	B	2012/03/01	15:05:15.87	46.036	12.341	13.0	2.0	78	19	13	0.4	0.6	0.16
4	B	2012/03/07	17:23:24.63	46.053	11.866	10.1	1.4	113	12	8	0.4	1.5	0.13
5	B	2012/04/02	23:25:12.43	46.049	12.125	10.1	1.3	114	16	11	0.9	1.4	0.29
6	B	2012/05/24	13:40:07.34	46.025	12.320	13.2	1.0	119	10	9	0.7	0.9	0.16
7	A	2012/09/15	00:40:17.84	45.913	12.225	10.0	1.1	128	13	11	0.7	0.6	0.17
8	B	2012/11/26	11:01:27.45	45.753	12.093	7.9	1.7	243	13	12	1.1	1.3	0.23
9	B	2012/12/18	19:58:01.80	45.775	12.280	4.7	1.7	261	13	11	1.2	1.6	0.25
10	B	2013/02/14	08:00:14.64	45.985	12.469	12.5	1.2	219	12	11	0.9	0.7	0.20
11	B	2013/05/02	15:37:53.00	46.071	12.375	12.2	2.2	55	23	17	0.5	0.8	0.20
12	B	2013/07/04	04:13:31.95	45.875	11.934	13.7	2.4	105	21	9	0.5	0.5	0.13
13	A	2013/10/03	03:39:20.78	45.900	12.193	8.4	1.0	63	14	10	0.5	0.6	0.17
14	B	2013/10/03	04:43:49.64	46.036	11.841	11.1	1.6	69	18	15	0.9	3.1	0.52
15	B	2013/12/05	09:31:14.64	45.932	12.335	6.9	1.2	267	11	9	0.6	0.6	0.10
16	A	2014/04/27	22:05:49.50	45.793	12.088	7.0	1.2	220	14	7	0.7	0.6	0.14
17	A	2014/05/01	13:26:24.01	45.880	12.196	9.6	1.4	88	13	11	0.6	0.6	0.17
18	A	2014/06/13	05:14:30.64	45.898	12.102	12.2	1.4	96	14	10	0.3	0.3	0.07
19	B	2014/07/07	10:50:38.70	45.993	12.215	15.1	2.9	78	23	10	0.5	0.6	0.16
20	B	2014/08/03	20:16:41.36	45.921	11.942	12.2	1.6	106	21	8	0.6	1.2	0.15
21	A	2014/10/06	17:56:56.10	45.938	12.156	12.5	1.1	103	14	12	0.4	0.5	0.13
22	B	2014/10/18	07:16:22.27	46.147	12.300	13.2	1.9	69	19	9	0.2	0.5	0.09
23	B	2015/01/28	17:09:18.36	46.143	12.113	15.7	2.6	66	19	6	0.5	0.9	0.15
24	A	2015/05/15	11:33:43.00	45.872	12.067	14.4	2.0	110	21	15	0.6	0.8	0.24
25	B	2015/07/10	00:41:29.38	45.863	11.973	13.7	2.0	83	23	7	0.5	0.7	0.20
26	B	2015/08/22	02:09:41.25	45.882	11.913	13.1	2.3	80	29	7	0.5	0.8	0.23
27	B	2016/05/05	17:41:43.84	46.166	12.358	11.2	2.3	52	28	10	0.5	1.0	0.25
28	B	2016/05/11	19:24:56.66	45.814	11.866	15.0	2.2	106	21	9	0.5	1.0	0.21
29	B	2016/06/21	00:55:46.57	45.985	12.219	15.6	2.5	72	21	11	0.6	0.9	0.23
30	B	2016/10/20	20:23:24.72	46.104	11.950	10.4	2.4	65	19	10	0.6	2.3	0.27

contributed to its location (Table 1), 40 s of pre-event ambient noise included; when the S-wave arrival time is not picked, a theoretical value is estimated on the basis of the P-wave arrival time, earthquake location and $V_P/V_S = 1.77$ (Priolo et al., 2015a). Furthermore, to avoid possible P- and S-wave contamination by secondary wave arrivals (e.g., the Moho reflections observed by Bragato et al., 2011), we limit our analysis to the signals recorded at hypocentral distances within 80 km.

3. The method

3.1. Site response estimation

To evaluate the site response at the EV stations, we applied the generalized inversion technique (GIT; Andrews, 1986). This method can be viewed as an extension of the classic reference site spectral ratio (RSSR; Borcherdt, 1970). In the RSSR technique, the site response is calculated as the spectral ratio between recordings acquired at the site of interest and the seismograms recorded at a nearby rock site (the reference site). It is assumed that both the records from the reference site and the records from the sites of interest contain the same source and propagation effects and that the reference station is not affected by any site effects (i.e. the site amplification at the reference is assumed constant with frequency and equal to 1).

The GIT method allows the use of asynchronous recordings (i.e. no need of having all the seismograms of each earthquake simultaneously recorded at both the site of interest and the reference site) and turns out to be more robust and flexible than RSSR. Similar approaches have been performed in the past by other authors (e.g., among many others, Hua et al., 2013; Picozzi et al., 2017).

In this study, we perform a GIT analysis using the MATLAB package GITANES (GIT Analysis of Earthquake Spectra) developed by Klin et al. (2017). In GITANES we consider the source and the seismic response terms as the unknowns of the problem. The propagation term is estimated on the basis of the propagation model and the known location of the seismic source. In particular, we assume a 1D attenuation model for the S-waves, with parameters representative for Northeastern Italy: $V_S = 3.4$ km, and $Q_S = 160$ (Laurenzano and Priolo, 2008; Moratto et al., 2012).

To compute the site effects at he EV stations, we use the recordings of 48 events occurring at the regional scale (i.e., an area ranging from Central Italy to Germany) in the period 2014–2015 (Table S1 and Fig. S1) and spanning the magnitude range $3.1 \leq M \leq 4.4$. The earthquake recordings were downloaded from the OASIS database (Priolo et al., 2015b) for the EV stations and for the Varnada station (VARN) belonging to the OX network (Fig. 1a).

The frequency site response of the EV sites is shown in Fig. 2. Each site features a different amplification level, since the sensors are deployed in boreholes at different depths (Priolo et al., 2015a): the lowest amplification (less than one) is found for the deepest station ED01, whose seismometer is located at a depth of 155 m, while higher amplification values are found for all the other stations, which have seismometers at depths ranging between 5 and 33 m. The stations ED05, ED07, ED08, ED09 and ED10 are equipped with sensors located at approximately 14 m deep, featuring an evident notch at approximately 7–10 Hz. The presence of spectral notches, whose position depends on the sensor depth and the S-wave velocity above it, is another effect of the borehole installation on the site amplification curves; the notches are due to the interference of the upgoing wavefields with the downgoing wavefields reflected by Earth's surface.

3.2. Seismic source parameter estimation

The estimation of source parameters from microearthquake spectra is conditional on the adequate correction for path attenuation and site response effects. For the present analysis we use the parametric approach proposed by Zollo et al. (2014), in which the path attenuation and the site response effects, that modify the signal spectrum radiated by seismic sources, are parameterized through physical models. With

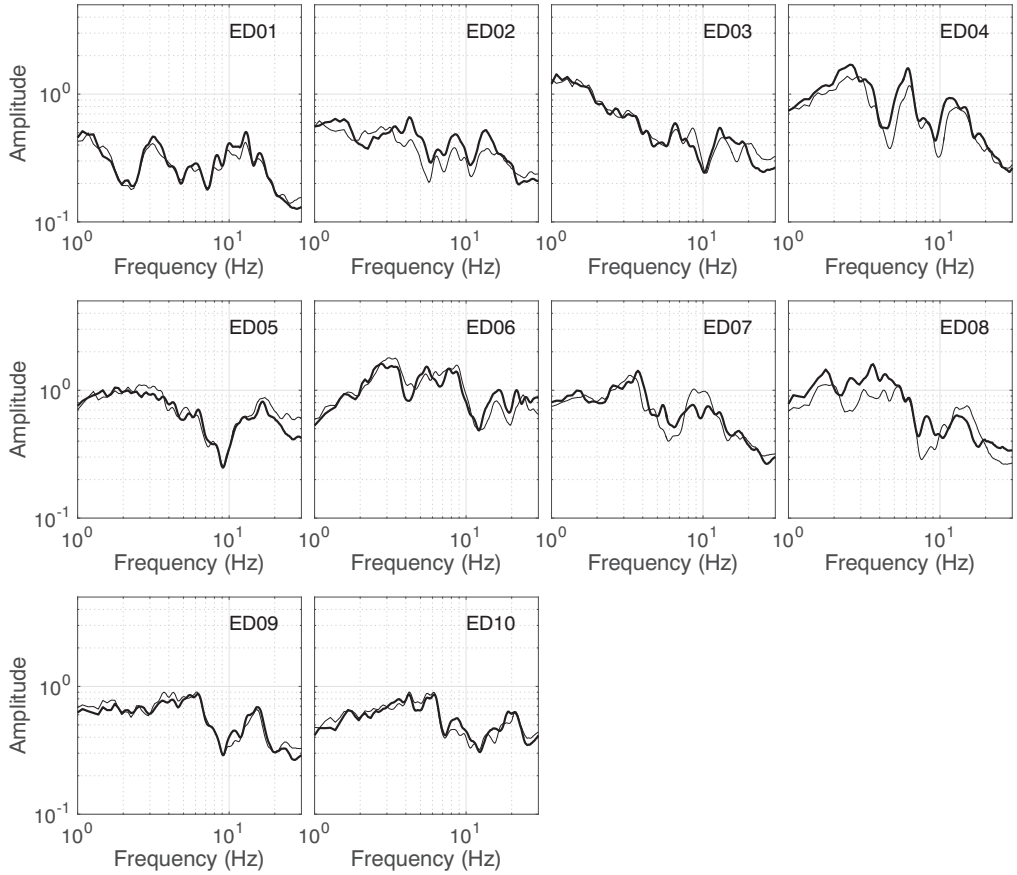

Fig. 2. Site response curves obtained by GIT for the two horizontal (EW thick and NS thin lines) components of the EV stations.

respect to non-parametric approaches, which are typically data-driven and need large set of data to properly describe the attenuation and site response effects, here the parametric approach, together with the use of a multistep, nonlinear inversion scheme, allows for accurate and robust estimations of seismic source parameters, path attenuation, and site amplification terms, also in case of reduced datasets or single event recordings.

In this study, we set the maximum frequency range for the inversion equal to 50 Hz to avoid noise at higher frequencies possibly related to anthropic sources; doing so, we stabilize the estimation of the corner frequency and reduce the related uncertainties. In addition, the observed signal-to-noise-ratio was used as a weighting factor for each individual record. Spectra from both the horizontal and vertical components of the S- and P-waves, respectively, were corrected for the site response by spectral deconvolution to obtain the source spectra. The site effects removal from a-priori information, leads the multistep, nonlinear inversion scheme to focus on the parameterization of the attenuation effects, which in turn leads to more accurate seismic source parameter estimates. In particular, the parametric model was tuned by a multistep iterative procedure that sets, for all source-receiver paths, the quality factor (Q_P and Q_S) and the parameter representing the high-frequency spectrum decay (γ). Once stabilized, the values of Q and γ were held fixed, and the source spectra were inverted to estimate the seismic moment (M_0) and the corner frequency (f_c). Finally, assuming the dynamic circular fault model (Madariaga, 1976), we estimated the source radius and the static stress drop for each considered earthquake, and we combined the source parameters with the radiated energy to evaluate both the apparent stress drop and the seismic efficiency. In particular, the seismic moment (M_0) is estimated from the low-frequency spectral level (Ω_0):

$$M_0 = C_s^{-1}\Omega_0 \tag{1}$$

where C_S is the distance-dependent parameter (Aki and Richards, 1980):

$$C_s = \frac{R_{\theta,\varphi}F_S}{4\pi\rho_h^{1/2}\rho_0^{1/2}c_h^{5/2}c_0^{1/2}R} \tag{2}$$

where $R_{\theta,\ \varphi}$ and F_S represent the radiation pattern coefficient and the free-surface factor, respectively, ρ is the density and c is the wave velocity estimated at the receiver (0) and the hypocenter depths (h). The geometrical spreading R is calculated (Ben-Menahem and Singh, 1981) as:

$$R = \sqrt{\frac{\rho_0 c_0}{\rho_h c_h}}\frac{X}{\sin j_k} \tag{3}$$

where X is the epicentral distance and j_k is the ray take-off angle. The moment magnitude (M_W) is computed from the seismic moment following Hanks and Kanamori (1979):

$$M_W = \frac{2}{3}(\log M_0 - 9.1) \tag{4}$$

The source radius (r) for the P- and S-waves is:

$$r = k_c\frac{c}{f_c} \tag{5}$$

where c is the wave velocity; f_c is the related corner frequency; $k_P = 0.32$ for P-waves; and $k_S = 0.21$ for S-waves. The static stress drop can be obtained as (Keilis-Borok, 1959):

$$\Delta\sigma = \frac{7}{16}\frac{M_0}{r^3} \tag{6}$$

while the apparent stress (τ_a) is (Wyss, 1979):

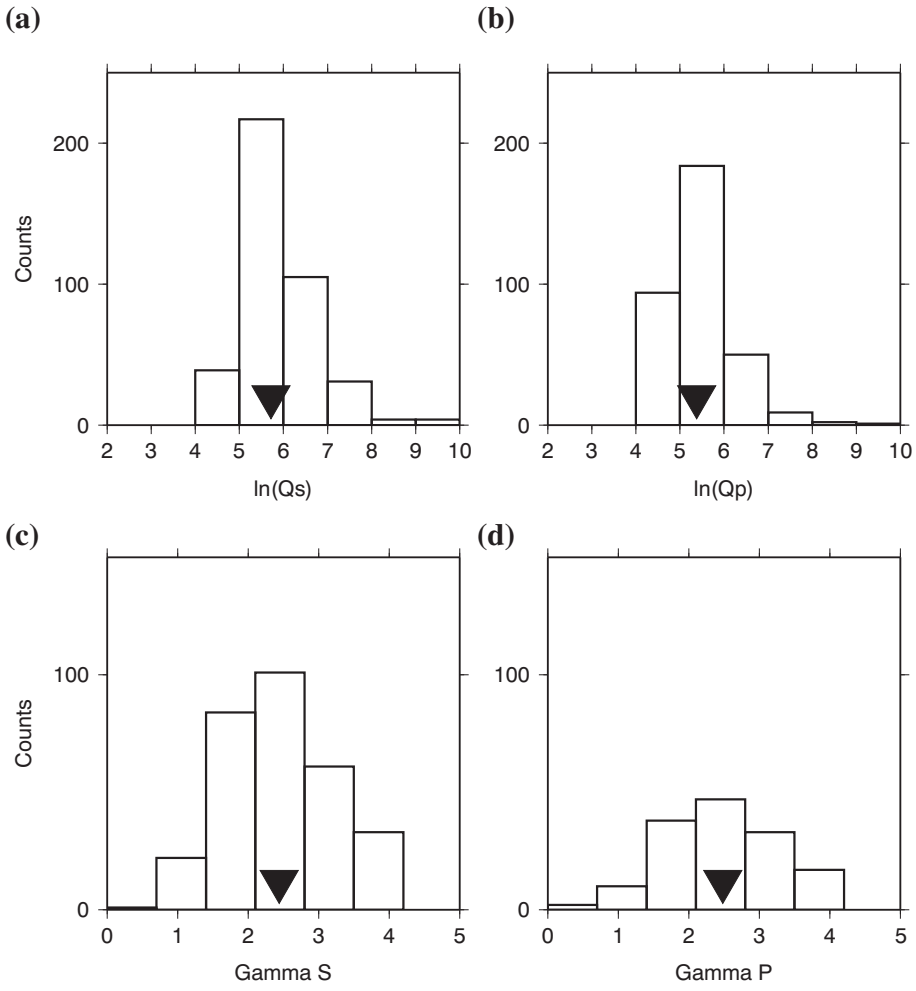

Fig. 3. (a) The distributions for Qs; (b) Qp; (c) γs; (d) γp obtained by the multistep iterative procedure with the related average values (black triangles).

$$\tau_a = \mu \frac{E_S}{M_0} \tag{7}$$

where μ is the crustal shear modulus and *Es* is the seismic radiated energy, which is computed as (Boatwrigth and Fletcher, 1984):

$$E_S = \frac{4\pi\rho c R^2}{F^2} \frac{1}{\pi} \int_0^\infty \omega^2 \, |U(\omega)|^2 \mathrm{d}\,\omega \tag{8}$$

where R represents the geometrical spreading, F is free-surface coefficient, c and ρ refer, to the velocity and the density of the propagation model, respectively; U(ω) is derived from the spectral model so we integrate in the whole frequency range the velocity spectrum represented by theoretical model to obtain more reliable results (Ide and Beroza, 2001). Finally, the Savage-Wood seismic efficiency (η_{SW}) is defined by Beeler et al. (2003):

$$\eta_{SW} = \frac{\tau_a}{\Delta\sigma} \tag{9}$$

We set the initial parameters for the inversion as follows: γ = 2.0, which is the standard value determined by Aki (1967) for the ω^{-2} spectrum; density ρ = 2700 kg/m^3, V_P = 6000 m/s, V_S = 3400 m/s, Qs = 160 and Qp = 400 in agreement with the velocity model proposed for the study area (Laurenzano and Priolo, 2008; Moratto et al., 2012); the ray take-off angles were calculated by using a gradient velocity distribution of V_S = 2230 + 0.08*z, which was retrieved from the EV reference 1D-model for the depth range 0–20 km; the reference value for the stress drop was set equal to 1 MPa (i.e., similar to Franceschina et al., 2006).

4. Results and discussion

We run the multistep procedure testing different values for the Q attenuation factor and the γ high-frequency spectrum decay; the model becomes stable after six iterations and the resulting Q and γ values are taken as references for the last step when the seismic moment and the corner frequency are estimated, respectively. The results of the iterative inversion procedure provide, for the attenuation model, a median value of Qs equal to 304 (i.e., 68% confidence limits of 169 and 740) and a mean value of γ = 2.44 ± 0.77 for S-waves, and a median value of Qp = 224 (121, 562) and γ = 2.48 ± 0.78 for P-waves (Fig. 3).

The distribution of Q estimates associated with various ray paths provides a first view on the spatial variations and 3D lateral heterogeneities of the seismic wave attenuation both for P- and S-waves. The resulting $Q_P/Q_S \approx 0.7$ is in contrast with the value expected for a theoretical Poisson solid ($Q_P/Q_S \approx 2.25$). Similar values (i.e., Qp < Qs) are very often observed in porous or densely fractured media permeated by fluids, as confirmed also by laboratory measurements (e.g., Toksoz et al., 1979; Morozov, 2015). Thus, the observed Qp/Qs ratio is a strong indicator of fluid presence in the investigated volume.

Regarding γ, the observed values (i.e., γ_s = 2.44 ± 0.77, γ_P = 2.48 ± 0.78) are, within the errors, slightly different from the fall-off slope of ω^{-2} according to Aki (1967). Since the ω^2 high-frequency fall-off is associated with an abrupt halt of the rupture at the circular border (Boatwright, 1988), the relatively high values of γ observed for the analyzed events may indicate a dominant deceleration mechanism for the rupture during the arrest phase. Deviation from the

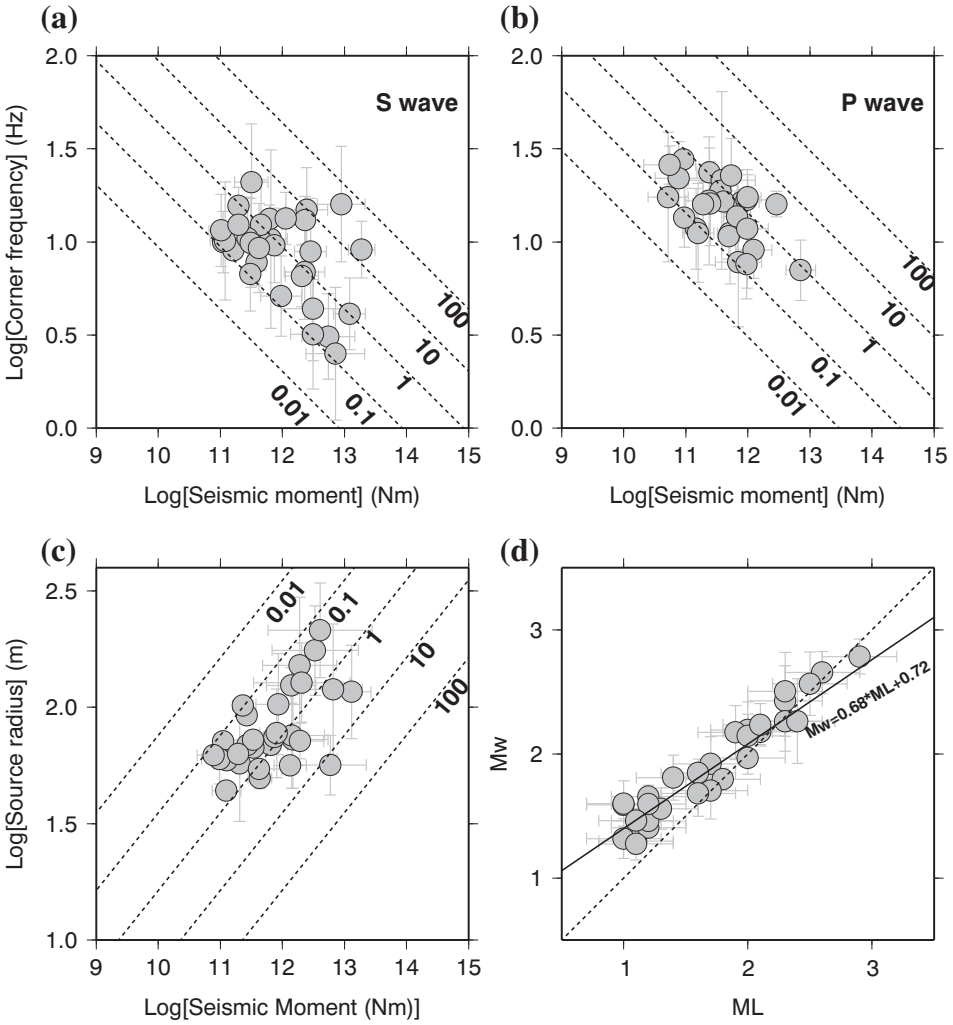

Fig. 4. a) f_c as a function of M_0 for S-wave source spectra, with related uncertainties, compared with constant $\Delta\sigma$ (dashed lines in MPa). b) Same as a) but for P-wave spectra. c) Source radius as a function of M_0, with related uncertainties, compared with $\Delta\sigma$ (dashed lines in MPa). d) M_W as a function of M_L compared with the relation (solid line) proposed by Moratto et al. (2017).

ω^2 model can also indicate that a source model with double corner frequencies could be more realistic as observed by Uchide and Kazutoshi (2016) who found fall-off exponent values slightly higher than 2.

The results for the source parameters are shown in Fig. 4. The seismic moment values span two orders of magnitudes for both S- and P-waves, with uncertainties < 0.3 for the large part of the considered earthquakes. M_0 derived from S-wave spectra ranges between $1{\cdot}10^{11}$ N·m and $5{\cdot}10^{13}$ N·m, while f_c varies between 2.5 Hz and 21 Hz. For the P-waves, M_0 ranges between $5{\cdot}10^{10}$ N·m and $7{\cdot}10^{12}$ N·m, and f_c varies between 7 Hz and 28 Hz (Fig. 4a–b). The uncertainties associated with f_c can be more relevant than the M_0 estimated by the long period part of the spectrum, and probably are connected to an unmodeled complexity of the source or uncorrected path effects and large azimuthal variability, possibly related to rupture directivity effects. Kaneko and Shearer (2015) demonstrated that a non-symmetrical circular model takes to a large variability in the estimated corner frequency owing to an increased azimuthal dependency due to asymmetric rupture evolution. Abercrombie (2015) calculated the corner frequencies using different sampling rate, showing that the corner frequency decreases as the high-frequency bandwidth limit decreases; in particular, the corner frequencies, falling within a factor of 3 in the high-frequency bandwidth limit, can be underestimated.

The source radius (R) ranges between 40 m and 215 m; its distribution versus seismic moment is scattered around a mean of 1 MPa (Fig. 4c). The distribution of the static $\Delta\sigma$ (derived from the source radius) ranges between 0.1 MPa and 15 MPa with a median value of 0.45 MPa and a confidence level of (0.2, 1.7), in agreement with previous studies done in the same area (e.g., Franceschina et al., 2006). To evaluate the accuracy of the stress drop is not easy since, being proportional to the cube of the corner frequency, the related uncertainty is tripled; several studies explained the possible causes of such high uncertainties (e.g. Kane et al., 2011; Abercrombie, 2015). Further, Prieto et al. (2007) considered that a 50% per cent error in stress drop can be realistic, and that the uncertainty can even increase considering possible errors in location and velocity models.

The M_L-M_W comparison shows that the two magnitudes correspond well in the range $2.0 \le M_W \le 3.0$ and that M_L systematically underestimates M_W for smaller earthquakes (Fig. 4d). These results are consistent with the relation proposed by Moratto et al. (2017), who estimated a M_L-M_W scaling ratio of 2/3 for northeastern Italy, and are also in agreement with the theory developed in previous studies (e.g. Hanks and Boore, 1984; Deichmann, 2018 and reference therein).

In Fig. 5a, we compare M_0 and Er, computed as the mean of the integral of the square ground motion velocity derived from the theoretical spectral model for each station and obtained by summing the P- and S-wave contributions. The energy associated with the S-waves (E_S) is larger than the energy associated with the P-waves (E_P), consistent

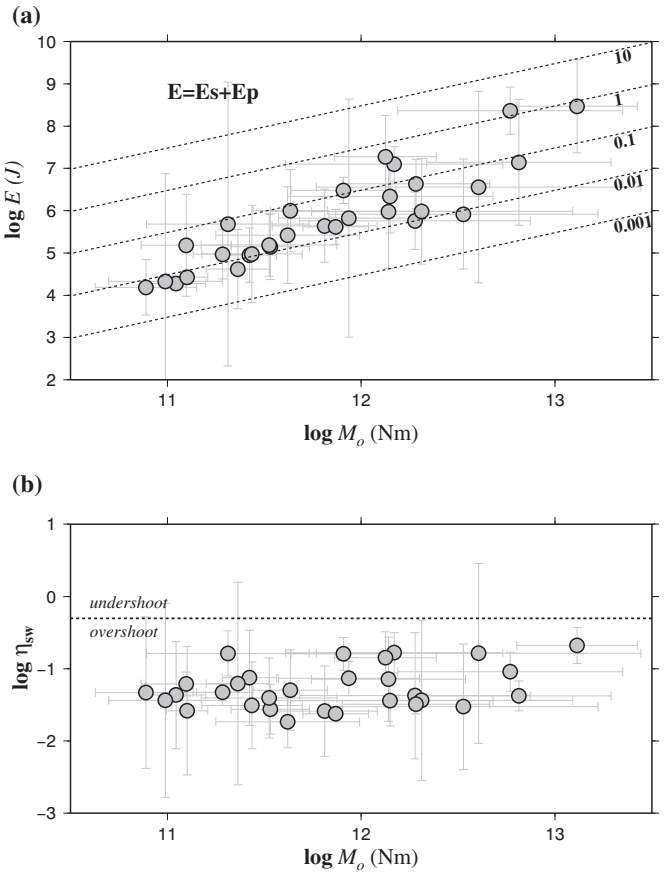

Fig. 5. a) Radiated energy versus seismic moment; the dashed lines indicate constant apparent stress drop (in MPa). b) Savage-Wood efficiency (η_{SW}) versus M_0; the threshold of 0.5 discriminates between the undershoot and overshoot mechanisms.

with Boatwright and Fletcher (1984) who estimated $E_S \approx 9{*}E_P$. In our study, the median of the E_S/E_P distribution is 19 (4–98 for the 68% confidence level) in agreement with Boatwrigth and Fletcher (1984). The seismic energy (Er) varies between 10^4 J and 10^9 J, while the apparent stress ranges between 0.005 and 0.5 MPa (Fig. 5a) with two larger earthquakes that reach the threshold of 1 MPa. Since the apparent stress drop is almost constant (Fig. 5a) over two orders of magnitude, M_0 and Er scale approximately constantly. The ratio between the apparent and the static stress drop is defined as the Savage-Wood seismic efficiency η_{SW} by Beeler et al. (2003). The efficiency is related to the comparison between the static and the dynamic stress drop, which is the difference between the yield stress and the dynamic friction stress. The rupture front activates the source process with an increase in the initial stress drop to a peak of yield stress generating a strength excess; when the source stops slipping, the stress decreases to the dynamic friction level, which can switch to a different final static stress drop value (Abercrombie and Rice, 2005).

In our case, the efficiency distribution (Fig. 5b) has a median value of 0.04 with confidence levels of (0.03, 0.14) and maximum and minimum values of 0.21 and 0.02, respectively. The dynamic and static stress drops are equal in the case of $\eta_{SW} = 0.5$; this threshold is useful to discern between overshoot (< 0.5) and undershoot (> 0.5) weakening dynamic processes (Beeler et al., 2003). Our values are all lower than 0.5 (Fig. 5b), meaning that the whole set of the analyzed sources features an overshoot dynamic mechanism. In each case, the uncertainty associated to the stress drop and caused by either the geometry or the rupture velocity influences also the radiation efficiency (Kaneko and Shearer, 2015). The estimated source parameters (M_W, stress drop and seismic efficiency) for the 30 analyzed events are not affected by their distance from the Collalto reservoir, as clearly shown in Fig. 6. Therefore, the UGS activity did not change the characteristics of the local background seismicity during the studied period.

The overshoot mechanism implies a dynamic stress drop lower than the static stress drop, and this situation is observed in many dynamic crack models (Madariaga, 1976). In this study, the apparent stress of 0.02 MPa is less than 10% of the static stress drop (0.45 MPa), so we can estimate an average dynamic stress drop of 0.24 MPa (Kanamori and Heaton, 2000). Following Beeler et al. (2003), the lower seismic efficiency leads to a positive overshoot value of 0.46, which manifests itself as slip velocities smaller than the cases related to similar magnitude earthquakes generated in laboratory or induced by mining; overshoot mechanisms can be related to high dynamic strength compared to the level of stress and can indicate that the final stress is lower than the overall strength of the fault (Meighan et al., 2014). In practice, our small seismic efficiency suggests that a very small fraction of the total energy available for the microearthquake rupture is converted into the radiated wave-field and, therefore, our values are consistent with laboratory observations of stick-slip faulting and elastodynamic fracture models (Beeler et al., 2003).

5. Conclusions

In this study, we estimated the source parameters (e.g., seismic moment and corner frequency) for a data set of 30 microearthquakes recorded around the Collalto UGS reservoir located in an area prone to natural earthquakes (Romano et al., 2019). The Montello-Collalto area is a densely populated area with lot of industries and historical heritage. From the seismotectonic point of view the area is highly representative of the compressional tectonic regime of the Southeastern Alpine front, with several damaging earthquakes occurred in the past and still many uncertainties about the geometry and seismogenic potential of the complex fault system present there, mostly buried beneath young sediments.

We apply the multistep procedure proposed by Zollo et al. (2014) further improved by the spectral correction of local site effects. The procedure was first tuned to a suitable set of seismic events with $1.0 \le M_L \le 2.9$ (i.e., $1.3 \le M_W \le 2.8$) located at depths of 5–15 km, and the waveforms were cleaned of path and site effects by deconvolution in the frequency domain. The effectiveness of the method applied (Zollo et al., 2014, integrated with site response correction) strongly depends on the quality of the network (good azimuthal coverage, very short interstation distance, good instrumental equipment, low seismic-to-noise ratio). Therefore, only by improving the quality of the monitoring infrastructures we may get useful information for discriminating natural from induced/triggered events.

The results show that M_0 (and consequently M_W) is well constrained, while f_c values are affected by larger uncertainties probably related to an unmodeled complex source (Kaneko and Shearer, 2015; Uchide and Kazutoshi, 2016) and uncorrected path effects. The static stress drop spans two orders of magnitude with an average value of 0.45 MPa, which can be a suitable reference for the microseismicity occurring in the study area; the apparent stress is less than 10% of the static stress drop, and all earthquakes show efficiency values compatible with overshoot processes, which is typical of natural (i.e., tectonic) earthquakes (Fig. 5b).

Furthermore, the apparent and static stress drops seem to scale with self-similar characteristics within one order of magnitude. We can also deduce that the energy radiated to the receivers is a fraction of the overall Er; the remaining energy could be dissipated in frictional heating or stored in the source becoming ready to generate new ruptures.

Our study improves the knowledge of the earthquakes that characterize the Southeastern Alps and provides an additional key of interpretation for the energy balance and the stress involved in microearthquake rupture processes. On the basis of the source parameters

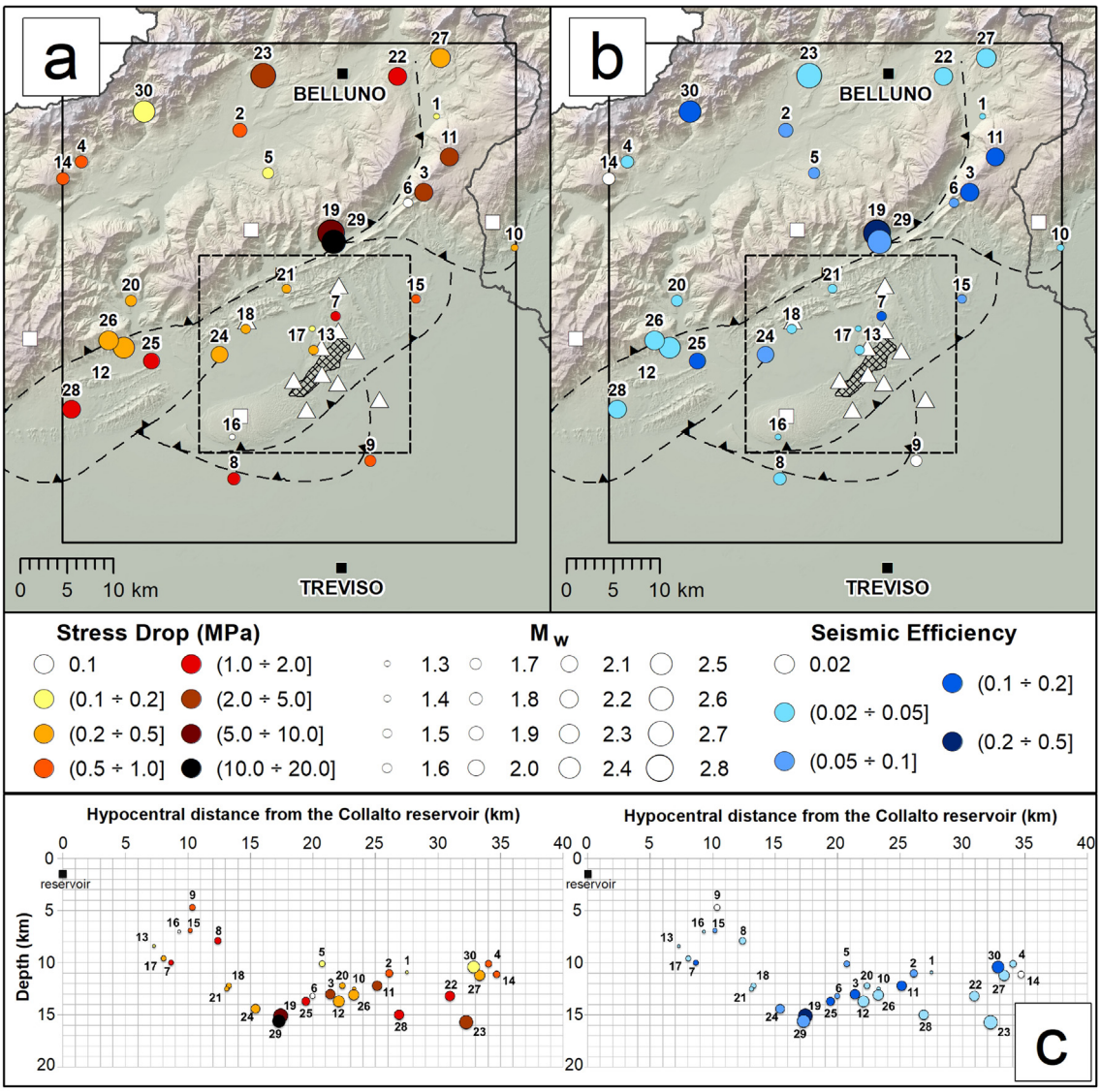

Fig. 6. Map of the 30 events (circles) analyzed in this study labeled with the ID number reported in Table 1. The radius of the circles is proportional to M_W and the color scale represents the stress drop values (a, c), and the seismic efficiency (b, c); c) Same events represented according to M_W, stress drop (left panel) and seismic efficiency values (right panel) with respect to depth and hypocentral distance from the Collalto reservoir.

estimated, there are no hints for which the seismicity recorded around the UGS activity of Collalto down to M_L 1.0 (i.e., M_W 1.3) can be regarded as induced. We cannot exclude that some micro-event below the detection capacity of the network - the magnitude of completeness has been estimated at M_L 0.3 for a 13 km wide volume surrounding the Collalto reservoir (Romano et al., 2019) - might be induced within or close to the reservoir. Nevertheless, the case analyzed in this study may be added to the few cases which document the low impact of UGS in depleted gas reservoirs with confining pressure not exceeding the original pressure in terms of induced seismicity (Evans, 2008).

We estimate a reference value for the stress drop of the microseismicity occurring in the study area and we evidence that all considered events have low seismic efficiencies consistent with stick-slip faulting and dynamic fracture processes. The investigated dataset consists of earthquakes of natural origin, being they located several km away from the Collalto gas reservoir and being the seismicity rate uncorrelated with the gas-pressure. However, such procedure is well feasible to investigate possible seismicity occurring close or in the Collalto reservoir and can provide a valuable information in the implementation of quasi real-time traffic-light protocols. Furthermore, the same strategy can be adopted in other active tectonic regions which host underground industrial activities potentially capable to trigger seismicity.

Supplementary data to this article can be found online at https://doi.org/10.1016/j.tecto.2019.04.030.

Acknowledgments

Editor-in-Chief Ramon Carbonell and three anonymous reviewers are acknowledged for their constructive comments, which helped in improving this article. The Collalto Seismic Network is managed by the OGS on behalf of Edison Stoccaggio S.p.A. under requirements of the Italian Ministry for the Environment, Land, and Sea Protection (MATTM) and in agreement with the Veneto Region. Seismic waveforms are from the EV (https://doi.org/10.7914/SN/EV) and OX (https://doi.org/10.7914/SN/OX) seismological networks. This study has been partly supported by the Italian Ministry for Economic Development (MiSE), General Directorate for Mining Resources, within the context of a Program Agreement with the OGS (n. 3835 of the Corte dei Conti under the activity “Development of analysis methods for a rapid correlation of the detected seismicity to the underground exploitation for energy production”) and the INSIEME project of the SIR-

MIUR program (grant no. RBSI14 MN31). Some figures were produced by the Generic Mapping Tool (Wessell and Smith, 1991).

References

Abercrombie, R.E., 2015. Investigating uncertainties in empirical Green's function analysis of earthquake source parameters. J. Geophys. Res. Solid Earth 120, 4263–4277.

Abercrombie, R.E., Rice, J.R., 2005. Can observations of earthquake scaling constrain slip weakening? Geophys. J. Int. 162, 406–424.

Aki, K., 1967. Scaling law of seismic spectrums. J. Geophys. Res. 72, 1217–1231.

Aki, K., Richards, P.G., 1980. Quantitative Seismology, Theory and Methods (2 Volumes). 932 pp.. W. H. Freeman, San Francisco.

Ameri, G., Emolo, A., Pacor, F., Gallovic, F., 2011. Ground-motion simulations for the M 6.9 Irpinia 1980 earthquake (southern Italy) and scenario events. Bull. Seismol. Soc. Am. 101, 1136–1151.

Andrews, D.J., 1986. Objective determination of source parameters and similarity of earthquakes of different size. In: Das, S., Boatwright, J., Scholz, C.H. (Eds.), Earthquake Source Mechanics. Am. Geophys. Union, Geophys. Monogr. Ser. 6pp. 259–267.

Avigliano, R., Poli, M.E., Zanferrari, A., 2008. Buried architecture of the Quaternary Vittorio Veneto basin (NE Italy). Boll. Geofis. Teor. Appl. 49 (3–4), 357–368.

Beeler, N.M., Wong, T.F., Hickman, S.H., 2003. On the expected relationships among apparent stress, static stress drop, effective shear fracture energy and efficiency. Bull. Seismol. Soc. Am. 93, 1381–1389.

Ben-Menahem, A., Singh, S.J., 1981. Seismic Waves and Sources, 1108 p. Springer-Verlag, New York.

Bindi, D., Spallarossa, D., Pacor, F., Picozzi, M., Scafidi, D., F. Cotton, F., 2018. Impact of magnitude selection on aleatory variability associated with ground-motion prediction equations: part I—local, energy, and moment magnitude calibration and stress-drop variability in Central Italy. Bull. Seismol. Soc. Am. 108, 1427–1442.

Boatwright, J., 1988. The seismic radiation from composite models of faulting. Bull. Seismol. Soc. Am. 78, 489–508.

Boatwrigth, J., Fletcher, J.B., 1984. The partition of radiated energy between P and S waves. Bull. Seismol. Soc. Am. 74, 361–376.

Borcherdt, R.D., 1970. Effects of local geology on ground motion near San Francisco Bay. Bull. Seismol. Soc. Am. 60, 29–61.

Bormann, P., Wendt, S., Di Giacomo, D., 2013. Chapter 3: seismic sources and source parameters. In: Bormann, P. (Ed.), New Manual of Seismological Observatory Practice (NMSOP-2). IASPEI, GFZ German Research Centre for Geosciences, Potsdam.

Bragato, P.L., Tento, A., 2005. Local magnitude in northeastern Italy. Bull. Seismol. Soc. Am. 95, 579–591.

Bragato, P.L., Sugan, M., Augliera, P., Massa, M., Vuan, A., Saraò, A., 2011. Moho reflection effects in the Po plain (Northern Italy) observed from instrumental and intensity data. Bull. Seismol. Soc. Am. 101, 2142–2152.

Brune, J., 1970. Tectonic stress and the spectra of seismic shear waves from earthquakes. J. Geophys. Res. 75, 4997–5009.

Burrato, P., Poli, M.E., Vannoli, P., Zanferrari, A., Basili, R., Galadini, F., 2008. Sources of Mw 5+ earthquakes in northeastern Italy and western Slovenia: an updated view based on geological and seismological evidence. Tectonophysics 453, 157–176. https://doi.org/10.1016/j.tecto.2007.07.009.

Choy, G.L., Boatwright, J., 1995. Global patterns of radiated seismic energy and apparent stress. J. Geophys. Res. 100, 205–226.

Deichmann, N., 2018. The relation between M_E, M_L and M_W in theory and numerical simulations for small to moderate earthquakes. J. Seismol. 22, 1645–1668.

Evans, D.J., 2008. An appraisal of underground gas storage technologies and incidents, for the development of risk assessment methodology - RR605 Research Report. Health and Safety Executive, UK Vol. 1 (264 pp.) and Vol. 2 (57 pp. + foreward and tables). http://www.hse.gov.uk/research/rrpdf/rr605.pdf, Accessed date: 20 March 2019.

Franceschina, G., Kravanja, S., Bressan, G., 2006. Source parameters and scaling relationships in the Friuli-Venezia Giulia (Northeastern Italy) region. Phys. Earth Planet. Inter. 154, 148–167.

Frankel, A., 1982. The effects of attenuation and site response on the spectra of microearthquakes in the Northeastern Caribbean. Bull. Seismol. Soc. Am. 72, 1379–1402.

Frankel, A., Wennerberg, L., 1989. Microearthquake spectra from the Anza, California seismic network: site response and source scaling. Bull. Seismol. Soc. Am. 79, 581–609.

Goertz-Allmann, B.P., Goertz, A., Wiemer, S., 2011. Stress drop variations of induced earthquakes at the Basel geothermal site. Geophys. Res. Lett. 38, L09308.

Grigoli, F., Cesca, S., Priolo, E., Rinaldi, A.P., Clinton, J.F., Stabile, T.A., Dost, B., Fernandez, M.G., Wiemer, S., Dahm, T., 2017. Current challenges in monitoring, discrimination, and management of induced seismicity related to underground industrial activities: a European perspective. Rev. Geophys. 55. https://doi.org/10.1002/2016RG000542.

Gruppo di Lavoro MPS, 2004. Redazione della mappa di pericolosità sismica prevista dall'Ordinanza PCM 3274 del 20 marzo 2003. In: Rapporto Conclusivo per il Dipartimento della Protezione Civile, INGV, Milano-Roma, aprile 2004, 65 pp. + 5 appendici.

Hanks, T.C., 1982. f max. Bull. Seismol. Soc. Am. 72, 1867–1879.

Hanks, T.C., Boore, D.M., 1984. Moment-magnitude relations in theory and practice. J. Geophys. Res. 89, 2033–2046.

Hanks, T.C., Kanamori, H., 1979. A moment magnitude scale. J. Geophys. Res. 84, 2348–2350.

Hua, W., Chen, A., Zheng, S., 2013. Source parameters and scaling relations for reservoir induced seismicity in the Longtan reservoir area. Pure Appl. Geophys. 170, 767–783.

Husen, S., Kissling, E., Deschwanden, A. von, 2013. Induced seismicity during the construction of the Gotthard Base Tunnel, Switzerland: hypocenter locations and source dimensions. J. Seismol. 17, 63–81.

ICHESE, 2014. Report on the hydrocarbon exploration and seismicity in Emilia Region. In: Paper Presented at International Commission on Hydrocarbon Exploration and Seismicity in the Emilia Region - ICHESE, (213 pp).

Ide, S., Beroza, G.C., 2001. Does apparent stress vary with earthquake size? Geophys. Res. Lett. 28, 3349–3352.

Kanamori, H., 1977. The energy release in great earthquakes. J. Geophys. Res. 82 (2981–2876).

Kanamori, H., Heaton, T.H., 2000. Microscopic and macroscopic physics of earthquakes. Geophys. Monogr. 120, 147–163.

Kanamori, H., Hauksson, E., Hutton, L.K., Jones, L.M., 1993. Determination of earthquake energy release and ML using TERRAscope. Bull. Seismol. Soc. Am. 83, 330–346.

Kane, D.L., Prieto, G.A., Vernon, F.L., Shearer, P.M., 2011. Quantifying seismic source parameter uncertainties. Bull. Seismol. Soc. Am. 101, 535–543.

Kaneko, Y., Shearer, P.M., 2015. Variability of seismic source spectra, estimated stress drop, and radiated energy, derived from cohesive-zone models of symmetrical and asymmetrical circular and elliptical ruptures. J. Geophys. Res. Solid Earth 120, 1053–1079.

Keilis-Borok, V.I., 1959. On the estimation of the displacement in an earthquake source and of source dimensions. Ann. Geophys. 12, 205–214.

Klin, P., Laurenzano, G., Priolo, E., 2017. GITANES: a MATLAB package for joint estimation of site spectral amplification and seismic source spectra with the generalized inversion technique. Seismol. Res. Lett. 89, 182–190.

Laurenzano, G., Priolo, E., 2008. Numerical modelling of earthquake strong ground motion in the area of Vittorio Veneto (NE Italy). Boll. Geofis. Teor. Appl. 49, 401–425.

Madariaga, R., 1976. Dynamics of an expanding circular fault. Bull. Seismol. Soc. Am. 66, 639–666.

Meighan, L.N., Urbancic, T., Baig, A., 2014. Seismic efficiency and overshoot of fractures associated with stimulation in heavy oil reservoirs. In: 76th EAGE Conference & Exhibition, 16–19 June 2014, Amsterdam (Netherlands).

MiSE, 2014. Guidelines for monitoring seismicity, ground deformation and pore pressure in subsurface industrial activities. http://unmig.mise.gov.it/unmig/agenda/upload/151_238.pdf, Accessed date: 30 August 2016.

Moratto, L., Suhadolc, P., Costa, G., 2012. Finite-fault parameters of the September 1976 M > 5 aftershocks in Friuli (NE Italy). Tectonophysics 536-537, 44–60.

Moratto, L., Saraò, A., Priolo, E., 2017. Moment magnitude (M_W) estimation of weak seismicity in Northeastern Italy. Seismol. Res. Lett. 88, 1455–1464.

Morozov, I.B., 2015. On the relation between bulk and shear seismic dissipation. Bull. Seismol. Soc. Am. 105, 3180–3188.

OGS - Istituto Nazionale di Oceanografia e di Geofisica Sperimentale, 2012. Collalto Seismic Network - Rete Sismica di Collalto. International Federation of Digital Seismograph Networks. Other/Seismic Network (10.7914/SN/EV).

OGS - Istituto Nazionale di Oceanografia e di Geofisica Sperimentale, 2016. North-East Italy Seismic Network. International Federation of Digital Seismograph Networks. Other/Seismic Network. 10.7914/SN/OX.

Ogwari, P.O., Horton, S.P., Ausbrooks, S., 2016. Characteristics of induced/triggered earthquakes during the startup phase of the guy-greenbrier earthquake sequence in north-central Arkansas. Seismol. Res. Lett. 87, 620–630.

Picozzi, M., Oth, A., Parolai, S., Bindi, D., De Landro, G., Amoroso, O., 2017. Accurate estimation of seismic source parameters of induced seismicity by a combined approach of generalized inversion and genetic algorithm: application to the Geysers geothermal area, California. *J. Geophys. Res. Solid* Earth 122, 3916–3933.

Prieto, G.A., Thomson, D.J., Vernon, F.L., Shearer, P.M., Parker, R.L., 2007. Confidence intervals for earthquake source parameters. Geophys. J. Int. 168, 1227–1234.

Priolo, E., Romanelli, M., Plasencia Linares, M., Garbin, M., Peruzza, L., Romano, M.A., Marotta, P., Bernardi, P., Moratto, L., Zuliani, D., Fabris, P., 2015a. Seismic monitoring of an underground natural gas storage facility: the Collalto seismic network. Seismol. Res. Lett. 86, 109–123.

Priolo, E., Laurenzano, G., Barnaba, C., Bernardi, P., Moratto, L., Spinelli, A., 2015b. OASIS - the OGS archive system of instrumental seismology. Seismol. Res. Lett. 86, 978–984.

Romano, M.A., Peruzza, L., Priolo, E., Garbin, M., Picotti, V., Guido, F.L., Ponza, A., 2015. Preliminary imaging of active faults in the Montello-Collalto area (Southeastern Alps, Italy) by a high-sensitivity seismometric network. In: INQUA Focus Group on Paleoseismology and Active Tectonics. 27. Miscellanea INGV, pp. 410–413.

Romano, M.A., Peruzza, L., Garbin, M., Priolo, E., Picotti, V., 2019. Microseismic portrait of the Montello thrust (Southeastern Alps, Italy) from a dense, high-quality seismic network. Seismol. Res. Lett (under review).

Rovida, A., Locati, M., Camassi, R., Lolli, B., Gasperini, P., 2016. CPTI15, the 2015 Version of the Parametric Catalogue of Italian Earthquakes. Istituto Nazionale di Geofisica e Vulcanologiahttps://doi.org/10.6092/INGV.IT-CPTI15.

Toksoz, M.N., Johnsont, D.H., Timur, A., 1979. Attenuation of the seismic wave in dry and saturated rocks. Laboratory experiments. Geophysics 44, 681–690.

Tusa, G., Brancato, A., Gresta, S., Malone, S.D., 2006. Source parameters of microearthquakes at Mount St Helens (USA). Geophys. J. Int. 166 (3), 1193–1223 1 September 2006.

Uchide, T., Kazutoshi, I., 2016. Small earthquakes deviate from the omega-square model as revealed by multiple spectral ratio analysis. Bull. Seismol. Soc. Am. 106, 1357–1363.

Wessell, P., Smith, W.H.F., 1991. Free software helps map and display data. Eos. Trans. AGU 72, 441.

Wyss, M., 1979. Observation and Interpretation of Tectonic Strain Release Mechanisms. PhD thesis. Calif. Inst. of Technol, Pasadena.

Zollo, A., Orefice, A., Convertito, V., 2014. Source parameter scaling and radiation efficiency of microearthquakes along the Irpinia fault zone in southern Apennines, Italy. J. Geophys. Res. Solid Earth 119. https://doi.org/10.1002/2013JB010116.